THE JOURNAL OF PHYSICAL CHEMISTRY B

ARTICLE

pubs.acs.org/JPCB

Distance and Temperature Dependency in Nonoverlapping and Conventional Förster Resonance Energy-Transfer

Johanna Vuojola,*[,†,§] Iko Hyppänen,[‡,§] Marika Nummela,[†] Jouko Kankare,[‡] and Tero Soukka[†]

[†]Department of Biotechnology, University of Turku, FI-20520 Turku, Finland

[‡]Department of Chemistry, Laboratory of Materials Chemistry and Chemical Analysis, University of Turku, Vatselankatu 2, FI-20014 Turku, Finland

Supporting Information

ABSTRACT: Förster resonance energy-transfer (FRET) is a powerful and widely applied bioanalytical tool. According to the definition of FRET by Förster, for energy-transfer to take place, a substantial spectral overlap between the donor emission and acceptor excitation spectra is required. Recently also a phenomenon termed nonoverlapping FRET (nFRET) has been reported. The nFRET phenomenon is based on energy-transfer between a lanthanide chelate donor and a spectrally nonoverlapping acceptor and thus obviously differs from the conventional FRET, but the mechanism of nFRET and resulting implications to assay design have not been thoroughly examined. In this work, a homogeneous DNA-hybridization assay was constructed to study the distance and temperature dependency of both nFRET and conventional FRET. Capture oligonucleotides were labeled at the 5′-end with a Eu(III)-chelate, and these conjugates hybridized to complementary tracer oligonucleotides labeled with an organic fluorophore at various distances from the 3′-end. The distance dependency was studied with a fluorometer utilizing time-resolution, and the temperature dependency was studied using a frequency-domain (FD) luminometer. Results demonstrated a difference in both the distance and temperature dependency between conventional FRET and nFRET. On the basis of our measurements, we propose that in nFRET thermal excitation occurs from the lowest radiative state of the ion to a higher excited state that is either ionic or associated with a ligand-to-metal charge-transfer state.

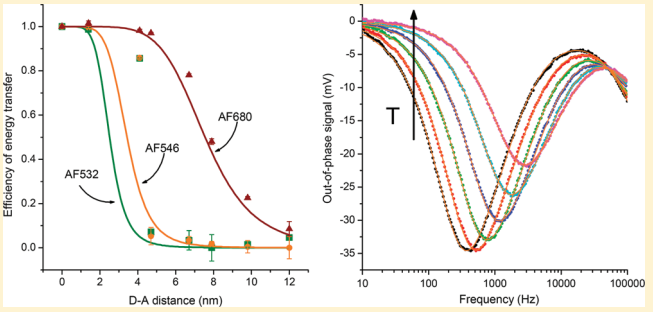

INTRODUCTION

Förster resonance energy-transfer is a physical process where an excited fluorescent donor transfers energy via a nonradiative dipole−dipole mechanism to a suitable acceptor in close proximity. The theoretical basis of the phenomenon was first introduced in 1948[1] and has since been widely applied.[2,3] The definition of FRET states that for energy-transfer to take place, a substantial spectral overlap is required between the donor emission and acceptor excitation spectra. Another requirement is a close proximity between the labels. FRET has been determined to be the prevailing mechanism in a distance range of approximately 1−10 nm.[1,4,5]

Recently a phenomenon termed nonoverlapping FRET (nFRET) has been reported with europium and samarium lanthanides.[6−8] The nFRET phenomenon is based on nonradiative energy-transfer between a lanthanide chelate donor and a spectrally nonoverlapping acceptor, meaning that the acceptor is excited at a higher energy level than where the donor has its main emittive transitions ($^5D_0 \rightarrow {}^7F_J$). Thereby also the energy-transfer enhanced emission of the acceptor can be measured at shorter wavelengths than where the emission of the donor is observed. Consequently nFRET helps to avoid the background originating from reabsorption of donor emission by the acceptor and from direct donor emission at the wavelength used to measure the acceptor emission.

Lanthanide chelates have frequently been used as donors in energy-transfer applications.[9−12] The chelate structure provides a scaffold for conjugation to biomolecules and also displaces water thus minimizing the O−H-vibration mediated quenching. The benefits of lanthanide chelates compared to traditional organic fluorophores include a substantial Stokes' shift that extends to several hundred nanometers and thus prevents excitation light scattering from interfering with the detection. Furthermore, the long millisecond scale emission decay of the lanthanide ions also increases the energy-transfer enhanced emission lifetime of a short lifetime acceptor. This enables the use of time-resolved fluorometry allowing the measurement of energy-transfer enhanced acceptor emission by gating out excitation light scattering and the nanosecond time scale background fluorescence originating from autofluorescence and directly excited acceptor molecules.[10,13]

Received: June 14, 2011
Revised: October 17, 2011
Published: October 18, 2011

ACS Publications © 2011 American Chemical Society

Table 1. Sequences of the Oligonucleotides

name of the oligo	sequence in 5′−3′ direction
capture	[b]CGG ATG ATG CGA GGC AAT GTA GGC TGA CAG ACA GAC CTG
tracer(1.4)[a]	CAG GTC TGT CTG TCA GCC TAC ATT GCC TCG CAT CAT[c] CCG
tracer(4.1)[a]	CAG GTC TGT CTG TCA GCC TAC ATT GCC TCG CAT[c] CAT CCG
tracer(4.7)[a]	CAG GTC TGT CTG TCA GCC TAC ATT GCC T[c]CG CAT CAT CCG
tracer(6.7)[a]	CAG GTC TGT CTG TCA GCC TAC AT[c]T GCC TCG CAT CAT CCG
tracer(7.9)[a]	CAG GTC TGT CTG TCA GCC T[c]AC ATT GCC TCG CAT CAT CCG
tracer(9.8)[a]	CAG GTC TGT CTG T[c]CA GCC TAC ATT GCC TCG CAT CAT CCG
tracer(12.0)[a]	CAG GT[c]C TGT CTG TCA GCC TAC ATT GCC TCG CAT CAT CCG

[a] The calculated distance in nanometers between the donor and the acceptor molecule.[16] [b] Terminal 5′-amino modification. [c] Amino-modified thymine.

Frequency-domain (FD) fluorometry is a method which can be used to accurately determine the lifetimes and intensities of fluorescent compounds.[14,15] In FD measurement a sample is excited with intensity modulated light resulting in the emission intensity being modulated at the same frequency. Due to the time lag between absorption and emission, there is a delay in the emission relative to the modulated excitation. The technique is well suited for the determination of lanthanide luminescence. The resolution of a complex decay requires measurements at a wide range of modulation frequencies. This range depends on the lifetimes of the species to be investigated. An appropriate range in the case of luminescent lanthanide chelates having a long lifetime is from 10 Hz to 100 kHz, which corresponds to lifetimes from 16 ms to 1.6 μs. The instrumentation in this time range is easily constructed by using a sine-wave modulated light source, such as a light emitting diode (LED), with moderate intensity as not to cause significant photochemical bleaching of the fluorophores. This frequency range also makes it possible to employ highly accurate and inexpensive digital lock-in amplifiers. Adding appropriate filters and a photomultiplier with a fast preamplifier, a complete FD luminometer can be relatively easily constructed.[15]

We report here a study of the distance and temperature dependency of conventional and nonoverlapping FRET using a homogeneous DNA-hybridization assay. We used Eu(III)-chelate labeled capture oligonucleotides and short-lifetime Alexa Fluor dye (AF) labeled tracer oligonucleotides that hybridized together to form an energy-transfer pair. In the nomenclature nonoverlapping indicates absence of spectral overlap between the Eu(III)-donor $^5D_0 \rightarrow {}^7F_J$ transitions and acceptor excitation spectrum. There is, however, an overlap with the very weak $^5D_1 \rightarrow {}^7F_J$ transitions. The term Anti-Stokes' shift FRET has also been used to describe the phenomenon, but the term nFRET was chosen to be used based on its previous usage in the publications describing the phenomenon.[6,7] The acceptors were chosen so that one (AF532) strictly followed the nFRET principle, one (AF680) strictly followed the conventional FRET principle, and one (AF546) had a very minor spectral overlap with the $^5D_0 \rightarrow {}^7F_J$ transitions and so might be able to partly utilize conventional FRET. The distance dependency was studied using a fluorometer. The close proximity between the donor and the acceptor label generated long-lifetime energy-transfer enhanced acceptor emission enabling time-resolved detection. The temperature dependency of conventional FRET and nFRET was studied using a modular FD luminometer in the low-frequency domain below 100 kHz.

EXPERIMENTAL METHODS

Chemicals and Materials. The capture oligonucleotides and the tracer oligonucleotides were purchased from Biomers.net GmbH (Ulm, Germany). The capture oligonucleotide contained a terminal 5′-amino modification. The tracer oligonucleotides had an internal amino-modified thymine base incorporated into the sequence at various distances from the 3′-end (Table 1). Both amino groups were at the end of a six-carbon linker. Both capture and tracer oligonucleotides were also purchased as an unmodified version to be used in excess as a blocker to prevent the hybridization of a labeled counterpart. The Alexa Fluor 532, 546, and 680 succinimidyl esters (AF532, AF546, and AF680) were from Molecular Probes (Eugene, OR). The helical structure of the DNA was taken into consideration when calculating the distances between the donor and the acceptor using a method described by Cardullo et al.[16] In the calculations, the length of the spacer was assumed to be 1.03 nm and the angle of the spacer from the normal of the helical axis was assumed to be 0 (spacer is perpendicular to the helical axis).

The used lanthanide chelates {2,2′,2″,2‴-{{4′-{4‴-[(4,6-dichloro-1,3,5-triazin-2-yl)amino]phenyl}-2,2′:6′,2″-terpyridine-6,6″-diyl}bis(methylenenitrilo)}tetrakis(acetato)}europium(III) (9d-DTA-chelate), {2,2′,2″,2‴-{[2-(4-isothiocyanatophenyl)-ethylimino]-bis(methylene)bis{4-{[4-(α-D-galactopyranoxy)phenyl]-ethynyl}-pyridine-6,2-diyl}bis(methylenenitrilo)}tetrakis(acetato)}-europium(III) (9d-ITC-chelate), and {2,2′,2″,2‴-{[4-[(4-isothiocyanatophenyl)ethynyl]pyridine-2,6-diyl]-bis(methylenenitrilo)}-tetrakis(acetato)}europium(III) (7d-ITC-chelate) (Figure 1) were synthesized following the protocols described earlier.[17−19] Sulforhodamine 101 used in the quantum yield studies was from Acros Organics (Geel, Belgium).

Labeling of Oligonucleotides with Eu(III)-Chelates and Alexa Fluor Dyes. The capture oligonucleotide containing a 5′-terminal amino-modification at the end of a six-carbon linker (Table 1) was labeled at the 5′-end with three different Eu(III)-chelates: 9d-ITC-, 9d-DTA-, or 7d-ITC-chelate (Figure 1). In the case of the 9d-ITC- and 7d-ITC-chelates, the capture oligonucleotide (5 nmol) and a 60-fold molar excess of the Eu(III)-chelate were dissolved into a total volume of 30 μL of 50 mM carbonate buffer pH 9.8. In the case of the 9d-DTA-chelate 15-fold molar excess in a total volume of 100 μL was used. The tracer oligonucleotides were labeled with Alexa Fluor succinimidyl ester dyes (AF532, AF546, and AF680) using the internal amino-modification at the end of a six-carbon linker on a thymine base incorporated into the sequence at various distances from the 3′-end (Table 1). In the labeling reaction the tracer oligonucleotide (5 nmol) and a 10-fold molar excess of the dye were dissolved into 50 μL of 100 mM carbonate buffer pH 9.2. All of the labeling reactions were incubated overnight at +37 °C protected from light. The capture oligonucleotide labeling reactions were incubated stationary, whereas the tracer oligonucleotide

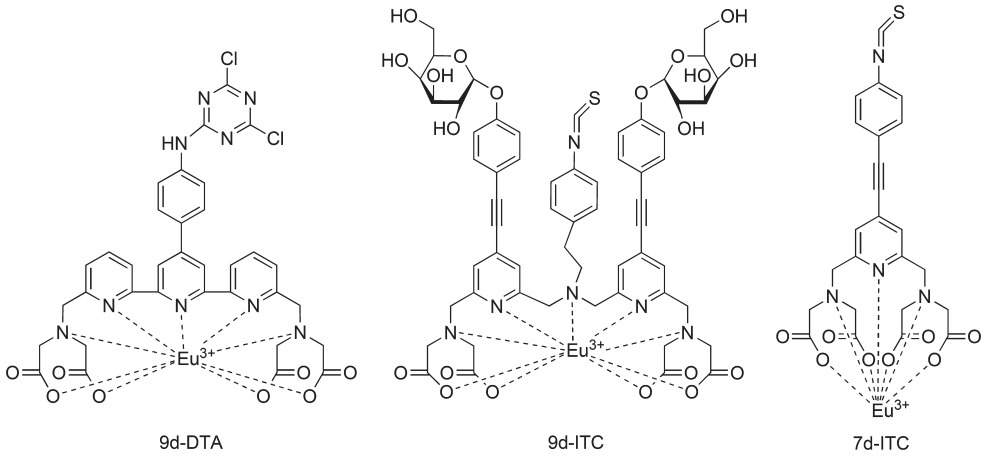

Figure 1. Structures of the used Eu(III)-chelates: 9d-DTA-chelate, 9d-ITC-chelate, and 7d-ITC-chelate.

labeling reactions were incubated in a 6 rpm rotation. The labeled oligonucleotides were isolated with reverse-phase HPLC (SpectraSYSTEM, Thermo Fisher Scientific) with a Phenomex Luna column (5 μm, 100 Å, 150 × 4.6 mm, C18) using an acetonitrile gradient. The pure fractions were dried in a vacuum concentrator (Hetovac CT 60e, Heto-Holten A/S, Allerød, Denmark), dissolved into TE buffer (10 mM Tris pH 8.0 containing 50 μM EDTA) and stored at −20 °C until further use.

Characterization of the Labeled Oligonucleotides. The chelate concentration of the labeled capture oligonucleotides was determined with the DELFIA system using Victor 1420 Multilabel Counter (PerkinElmer Life and Analytical Sciences, Wallac Oy, Turku, Finland) by comparing the fluorescence signal from the lanthanide ion (dissociated from the original chelate and captured by a secondary chelate present in the enhancement solution) to the signal obtained from a known concentration of Eu(III)-standard (PerkinElmer Life and Analytical Sciences). The dye concentration of the labeled tracer oligonucleotides and the oligonucleotide concentration of the capture and tracer oligonucleotides was determined with the NanoDrop ND-1000 spectrophotometer (Thermo Fisher Scientific, Waltham, MA). Absorption measurements were made at 520 nm for the AF532 (extinction coefficient of 81 000 M^{-1} cm^{-1}), at 556 nm for the AF546 (104 000 M^{-1} cm^{-1}), at 679 nm for the AF680 (184 000 M^{-1} cm^{-1}), and at 260 nm for the oligonucleotide. The absorbance of the label component present at 260 nm was estimated from the absorption spectrum and used for correction.

Spectral Measurements. The spectral measurements were performed with a Varian Cary Eclipse fluorescence spectrophotometer (Varian Scientific Instruments, Mulgrave, Australia). The samples were diluted in 50 mM Tris-HCl pH 8.0 containing 600 mM NaCl and 0.01% (v/v) Tween 20 to a concentration of 144 nM for the capture and 216 nM for the tracer oligonucleotide in a total volume of 100 μL (the labeled oligonucleotide hybridized to an unlabeled complementary oligonucleotide). The hybridization was allowed to take place for 1 h at 37 °C protected from light followed by dilution of the sample with 200 μL of buffer resulting in a final concentration of 48 nM for the capture oligonucleotide and 72 nM for the tracer oligonucleotide. The measurements were done in room temperature. The acceptor excitation spectra were measured utilizing the fluorescence mode of the instrument. The used emission wavelengths were 559 nm for AF532, 579 nm for AF546, and 713 nm for AF680 with 20 nm emission slit and 2.5 nm excitation slit. The donor emission spectra were measured utilizing the phosphorescence mode of the instrument with 100 μs delay and 700 μs gate time using an excitation wavelength of 340 nm (5 nm emission slit and 20 nm excitation slit). To visualize the weak $^5D_1 \rightarrow {}^7F_J$ transitions of the 9d-DTA-chelate, the emission spectrum was also measured from 1 μM solution of unconjugated chelate with the same measurement protocol.

Energy-Transfer Efficiency. The difference in the donor−acceptor distance dependency between conventional FRET and nFRET was studied by comparing the energy-transfer efficiency in samples containing hybridized oligonucleotides with a varying donor−acceptor distance. Measurements were made in triplicate in yellow LowFluor MaxiSorp microtitration wells (Nunc, Roskilde, Denmark). The used assay conditions and parameters were optimized in terms of the buffer composition, oligonucleotide concentration, oligonucleotide ratio, hybridization temperature, measurement delay, measurement gate time, and the used emission filters. The optimized hybridization reactions contained 12 nM capture oligonucleotide and 18 nM tracer oligonucleotide (1.5-fold molar excess) in 50 mM Tris-HCl pH 8.0, 600 mM NaCl, 0.01% (v/v) Tween 20. As a radiative energy-transfer background control to study the reabsorption of donor emission by the acceptor, a mixture of 12 nM capture, 360 nM unlabeled tracer oligonucleotide (30-fold molar excess) and 18 nM tracer(12.0) was used. The reactions were incubated for 30 min at +37 °C protected from light. Fluorescence of the Eu(III)-chelates and the energy-transfer enhanced emission of the Alexa Fluor dyes were measured at room temperature with a Victor 1420 Multilabel Counter (Wallac Oy) using standard filters. In all cases the excitation was at 340 nm. For the Eu(III)-chelate measurements 615 nm emission filter, 400 μs delay and 400 μs measurement time was used. The energy-transfer enhanced emission of AF532 and AF546 was measured at 560 nm and the energy-transfer enhanced emission of AF680 at 730 nm. For all the energy-transfer measurements 60 μs delay and 50 μs measurement time was used.

Frequency-Domain Measurements. For the FD measurements, samples containing 100 nM capture oligonucleotide (9d-DTA) and 150 nM tracer oligonucleotide (AF532, AF546 or AF680) in 50 mM Tris-HCl pH 8.0, 600 mM NaCl, 0.01% (v/v) Tween 20 with a total volume of 80 μL were incubated at 37 °C for 1 h (in order to obtain sufficient signal intensity, tracer (4.1)

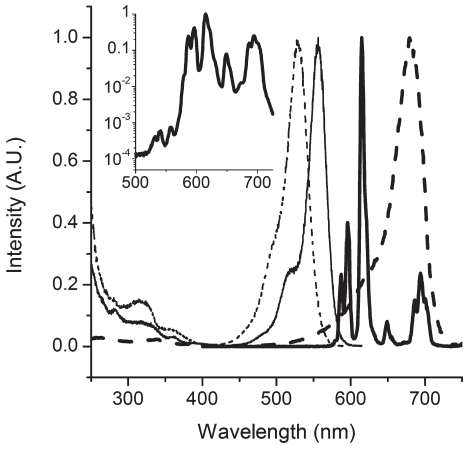

Figure 2. Normalized excitation spectra of the Alexa Fluor dyes 532 (narrow dashed line), 546 (narrow solid line), and 680 (thick dashed line) conjugated to tracer oligonucleotide and the normalized emission spectrum of the 9d-DTA-chelate (thick solid line) conjugated to capture oligonucleotide. In the inset, the emission spectrum of unconjugated 9d-DTA-chelate is depicted on a logarithmic scale (same axes as in the main picture).

was used with AF532 and AF546, and tracer (6.7) with AF680). As a control a reaction with capture oligonucleotide and unlabeled tracer oligonucleotide was prepared. The fluorescence lifetimes at different temperatures (5−55 °C) were measured with a modular frequency-domain (FD) luminometer. The instrument is described in a previous publication.[20] For compensating instrumental gain and phase shifts a LUDOX HS-40 (Sigma−Aldrich, St. Louis, MO) colloidal silica sample was measured at room temperature. In the LUDOX measurement the scattered excitation radiation was detected and on the emission chamber only optical density filters (FDI-2520 and FDI-2510, UQG Optics, Cambridge, England) were used to keep the intensity in suitable level for the photomultiplier. The sine-wave modulation degree of the excitation light was 70%. The detected emission wavelength was selected with an interference filter (615 nm with 8 nm fwhm, 560 nm with 10 nm fwhm or 730 nm with 10 nm fwhm). Luminescence was measured at 200 frequencies divided equidistantly in the logarithmic scale between 10 Hz and 100 kHz. The duration of one measurement was 25 min. The experimental data collected consisted of in-phase and out-of-phase signals of lock-in amplifier at the measurement frequencies. The fitting was done with out-of-phase signal only due to the in-phase interference caused by direct excitation of the acceptor dyes. Compensation with a LUDOX measurement was used in all fits. The goodness of fitting was estimated by the value of reduced Chi-square and randomness of Lag plots. The theory of the FD measurement and fitting is discussed in previous publications.[15,20]

RESULTS AND DISCUSSION

Spectral Measurements. The normalized excitation spectra of the Alexa Fluor dyes 532, 546, and 680 conjugated to tracer oligonucleotide and the normalized emission spectrum of the 9d-DTA-chelate conjugated to capture oligonucleotide are shown in Figure 2. The measured spectra were corrected for the wavelength sensitivity of the PMT. The inset in Figure 2 shows the time-gated donor emission spectrum measured from a concentrated solution of unconjugated chelate to visualize the low-intensity emission from the $^5D_1 \rightarrow {}^7F_J$ transitions of the Eu(III)-chelate donor around 530, 540, and 560 nm resulting from thermal excitation[20] (see the Theoretical Considerations section). The intensity of these peaks is more than 3 orders of magnitude smaller compared to that of the main peak at 615 nm.

The nFRET principle was demonstrated using Alexa Fluor 532 as the acceptor dye since it has no spectral overlap with the $^5D_0 \rightarrow {}^7F_J$ transitions of the Eu(III)-chelate donor. The conventional FRET was demonstrated using AF680 as the acceptor dye, which has a strong spectral overlap with the donor. In the case of AF546 dye, in principle both mechanisms are possible, since AF546 has a minor spectral overlap with the $^5D_0 \rightarrow {}^7F_0$ (visible with 9d-DTA-chelate at 587 nm) and the $^5D_0 \rightarrow {}^7F_1$ transition (at 596 nm for 9d-DTA-chelate or at 592 nm for 7d- and 9d-ITC-chelates). It has to be noted, however that the europium emission peak associated with the $^5D_0 \rightarrow {}^7F_1$ transition is defined to a magnetic dipole transition and cannot participate to Förster-type energy-transfer over a long distance.[21−23]

Energy-Transfer Efficiency. For the energy-transfer measurements the capture oligonucleotides conjugated to one of the three Eu(III)-chelates (9d-DTA, 9d-ITC, or 7d-ITC) were hybridized to tracer oligonucleotides conjugated to one of the three Alexa Fluor dyes (AF532, AF546 or AF680) with seven varying distances from the 3′-end, and the energy-transfer enhanced emission of the Alexa Fluor dyes was measured. In the absence of any mathematical model for the calculation of energy-transfer efficiency for the nFRET, the Förster model was applied for both nFRET and FRET reactions. This way it could also be seen whether there is a discrepancy between nFRET and the model.

Energy-transfer efficiency depends on the critical energy-transfer distance, or Förster radius (R_0). At R_0 the energy-transfer efficiency is 50%; that is, the rate of the energy-transfer is equal to the fluorescence decay rate. Förster radius on the other hand depends on the spectral properties of the donor and the acceptor as well as on the surrounding medium. The theoretical Förster radii (in Å) were calculated using the eq 1

$$R_0 = 0.211(JQ_D n^{-4}\kappa^2)^{1/6} \quad (1)$$

where J is the overlap integral of the fluorescence emission spectrum of the donor and the absorption spectrum of the acceptor, Q_D is the fluorescence quantum yield of the donor in the absence of the acceptor (see Supporting Information), n is the refractive index of the medium, and κ^2 is the factor related to the relative orientation in space of the transition dipoles of the donor and the acceptor molecule. The overlap integral is further defined as

$$J = \int_0^\infty F_D(\lambda)\varepsilon_A(\lambda)\lambda^4 \, d\lambda \quad (2)$$

where F_D is the corrected fluorescence emission spectrum of the donor with the total intensity normalized to unity and ε_A is the molar extinction coefficient of the acceptor in M^{-1} cm^{-1} at wavelength λ. The overlap integrals were calculated taking into account all the donor transitions, including the $^5D_1 \rightarrow {}^7F_J$ transitions and the $^5D_0 \rightarrow {}^7F_1$ magnetic dipole transition. The following values were used in the calculations: a refraction index (n) of 1.33 for water, an orientation factor (κ^2) of 2/3, and a quantum yield (Q_D) of 0.854, 0.603, and 0.182 for 9d-DTA-, 9d-ITC-, and 7d-ITC-chelates, respectively (see the Supporting

Table 2. Comparison of the Different Donor−Acceptor Pairs (D−A Pair) in the Hybridization Assay: Experimental Förster Radius (exp. R_0, See eq 3), Theoretical Förster Radius (Theor. R_0, See eq 1), Overlap Integral (J, See eq 2), Maximum Signal Divided by Respective Radiative Energy-Transfer Background Signal (max sg/bg), and Total Energy-Transfer Efficiency (exp. Q_{tot}, See eq 3)

D−A pair	exp. R_0 (nm)[a]	theor. R_0 (nm)	J (M^{-1} cm^{-1} nm^4)	max sg/bg	exp. Q_{tot} (%)[a]
9d-DTA/AF532	4.3	2.5	1.57×10^{13}	126	87
9d-DTA/AF546	4.6	3.4	1.02×10^{14}	1123	83
9d-DTA/AF680	7.7	7.6	1.15×10^{16}	125	79
9d-ITC/AF532	4.5	2.3	1.26×10^{13}	31	90
9d-ITC/AF546	4.6	3.3	1.17×10^{14}	707	88
9d-ITC/AF680	7.7	6.8	8.73×10^{15}	120	82
7d-ITC/AF532	4.5	1.9	1.52×10^{13}	47	95
7d-ITC/AF546	4.4	2.7	1.07×10^{14}	1140	92
7d-ITC/AF680	7.1	5.6	9.32×10^{15}	263	89

[a] Data obtained from europium emission at 615 nm.

Information). The orientation factor presents a source of error on the distance calculations since the factor 2/3 assumes a random orientation, such as free molecules in a low-viscosity solution. In the experimental setting, however, the acceptor and the donor were conjugated to oligonucleotides, which might hinder the free rotation. The orientation factor may be between 0 and 4, depending on the conditions, but in this case is limited between 1/3 and 4/3 since the used Eu(III)-chelates have unpolarized emission due to long lifetime (slow fluorescence decay).[5] After calculating the theoretical Förster radii, the theoretical energy-transfer efficiencies could be calculated using the eq 3

$$E = \frac{1}{1 + R^6/R_0^6} \tag{3}$$

where R is the donor−acceptor distance.

The experimental (observed) energy-transfer efficiencies were calculated using the eq 4

$$E = 1 - \frac{F_{DA}}{F_D} \tag{4}$$

where F_{DA} is the fluorescence intensity of the Eu(III)-chelate donor at 615 nm in the presence of the acceptor and F_D is the fluorescence intensity in the absence of the acceptor (unlabeled tracer oligonucleotide was used instead). The experimental Förster radii were then calculated using a fit based on eq 3. The total energy-transfer efficiency (Q_{tot}) representing the maximal donor quenching observed as the result of energy transfer was determined from the same fit.

The maximum signal-to-background ratio was determined by comparing the energy-transfer enhanced acceptor emission signals between a positive sample (Eu(III)-chelate labeled capture together with a dye labeled tracer) and a radiative energy-transfer background control (Eu(III)-chelate labeled capture together with a dye labeled tracer (12.0) and excess unlabeled tracer). When excess unlabeled tracer oligonucleotide is added, the background emission signal arises from radiative energy-transfer as opposed to nonradiative energy-transfer. First, the distance between the donor and the acceptor is defined by the diffusion of the labeled oligonucleotides, which in low concentrations leads to negligible nonradiative energy-transfer. Also the tracer (12.0) was chosen as it produces minimal nonradiative energy-transfer when hybridized to the capture oligonucleotide due to the long donor−acceptor distance. Furthermore, the components are separated by charge repulsion, because the oligonucleotide chains, the Eu(III)-chelates, and the Alexa Fluor dyes are all negatively charged.

Comparison of the different donor−acceptor pairs in the hybridization assay with relation to the aforementioned parameters is presented in Table 2. There was approximately 10-fold difference in the overlap integrals between the AF532 and AF546, and approximately 700-fold between the AF532 and AF680 acceptors. With the AF680 the theoretical R_0 values calculated from the measured overlap integral and donor quantum yield were in the expected range of approximately 6−7 nm depending on the used chelate and there was a clear difference between the theoretical R_0 values of the AF532 and AF546 acceptors. In the experimental R_0 values with AF680 the Förster radius was again in the expected range of approximately 7 nm. However, the experimental R_0 values of AF532 and AF546 acceptors were notably greater than the corresponding theoretical R_0 values and there was no difference between the experimental R_0 values of AF532 and AF546 acceptors. Thus, with AF546 and most notably with AF532 acceptor the energy-transfer is more efficient than would be expected based on the Förster mechanism and the results cannot be explained solely by this mechanism. The margins of error in experimental R_0 were in the range of 0.6−2.1%. With high acceptor concentrations radiative background causes a problem in applications based on conventional FRET when using a highly sensitive approach, such as time-resolved measurement. This could clearly be seen when comparing the maximum signal-to-background ratios using AF546 and AF680. The lower signal-to-background ratios with AF532 were the result of gating since efficient energy-transfer shortened the lifetime of the emission and led to reduction of the signal with the selected measurement parameters. The total energy-transfer efficiencies were in the range of 79−95% with the margins of error in the range of 0.2−1.0%. The best quenching percentage was obtained with the nFRET acceptor AF532 and the least quenching was observed with the FRET acceptor AF680. There were small differences between the used donor oligonucleotide conjugates, which is partly explained by variation in the small amount of free Eu(III)-chelate remaining in the fractions after HPLC-purification. It has to be noted that there are some uncertainties regarding the calculations of the energy transfer efficiency through donor quenching (see eq 4) since this method suffers for example from the above-mentioned small portion

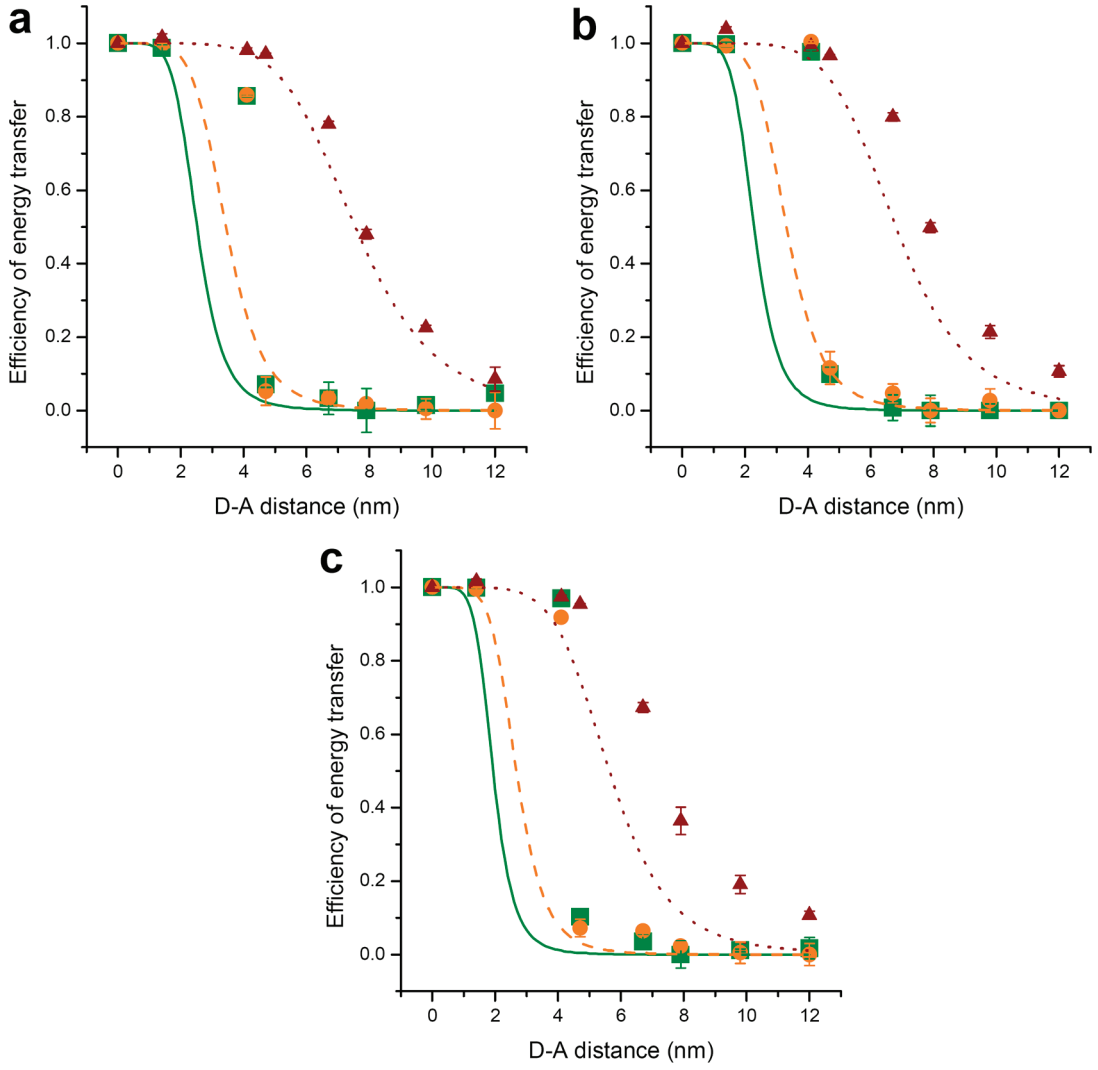

Figure 3. Comparison of the theoretical energy-transfer efficiencies (lines; calculated based on spectral overlapping) and actual experimental (symbols) energy-transfer efficiencies of different donor−acceptor pairs. The used Eu(III)-chelate donors were (a) 9d-DTA-chelate, (b) 9d-ITC-chelate and (c) 7d-ITC-chelate. The used acceptors were AF532 (green solid line, square), AF546 (orange dashed line, circle) and AF680 (red dotted line, triangle). The error bar represents the standard deviation between three replicate reactions. With AF532 and AF546 especially at the distance of 4.1 nm the experimental energy-transfer efficiency is substantially greater than the theoretical value.

of free Eu(III)-chelate, from possible secondary structures of the DNA preventing complete quenching and from nonoptimal measuring equipment unable to record very short-lived emission.

In Figure 3 the theoretical and experimental energy-transfer efficiencies are presented in relation to the donor−acceptor distance. The theoretical calculations were done using the eq 3, and they gave a continuous line. The symbols represent the experimental measurement results and they were calculated from the measurement signal at 615 nm using the eq 4. The data were normalized in relation to the exp. Q_{tot} (see Table 2). From Figure 3 it can be seen that when the D−A distance extends from 4.1 to 4.7 nm the energy transfer efficiency with the FRET acceptor AF680 remains high, whereas with the other two acceptors, the energy transfer efficiency declines very rapidly. With AF680 the experimental results follow the theoretical energy transfer efficiency, but with AF532 and AF546 especially at the distance of 4.1 nm the experimental energy-transfer efficiency clearly deviates from the theoretical value being considerably more effective than what could be expected based on the Förster theory. This indicates a distance dependency greater than $1/R^6$. With all the D−A distances the systematic discrepancy between the theoretical and experimental values (most prominent in Figure 3c) is most likely an effect of the used quantum yield value (Q_D, see eq 1), that greatly effects the horizontal position of the theoretical line. The determination of the Q_D with the 7d-ITC-chelate thus seems to have been the least accurate.

Frequency-Domain Measurements. With the FD method, the relatively large number of modulation frequencies allows an accurate determination of lifetimes and corresponding amplitudes and the main advantage of the frequency-domain methods compared to time-domain methods is generally considered to be the more accurate determination of multiple lifetimes. The influence of temperature to FRET and nFRET lifetimes was studied using FD measurements. The emission from reactions containing 100 nM capture oligonucleotide (9d-DTA) and 150 nM labeled or unlabeled tracer oligonucleotide was measured at 560 (AF532/AF546), 730 (AF680), or 615 nm (control with 9d-DTA chelate labeled capture oligonucleotide and unlabeled tracer oligonucleotide). In Figure 4

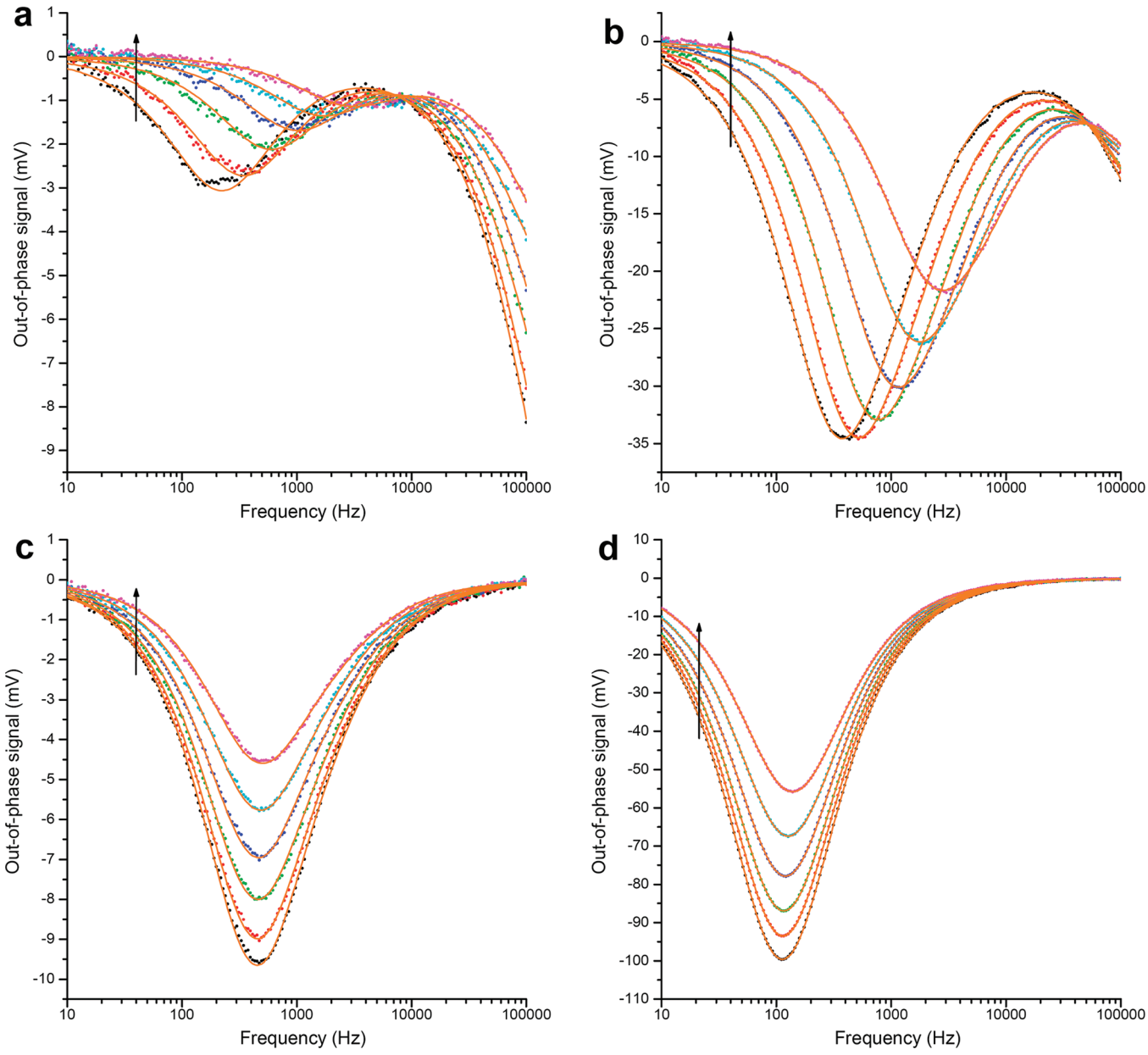

Figure 4. Out-of-phase signals of the emission from hybridization reactions containing 9d-DTA donor oligonucleotide together with a tracer oligonucleotide labeled with (a) AF532 acceptor, (b) AF546 acceptor, (c) AF680 acceptor, or (d) no acceptor at 560, 560, 730, and 615 nm, respectively, are shown as a function of modulation frequency in different temperatures. In order to obtain sufficient signal intensity, tracer(4.1) was used with AF532 and AF546, and tracer (6.7) with AF680. The experimental points are marked by circles, and the solid lines are the fitted signals with two (a, c, and d) or three (b) lifetimes (see Table 3). The temperatures ranged from 5 to 55 °C with 10 °C intervals. The arrow indicates increasing temperature.

the graphs of the out-of-phase signal of the lock-in amplifier are shown as a function of modulation frequency in different temperatures. The corresponding lifetimes are shown in Table 3. In Figure 5 the logarithm of the kinetic constants $(1/\tau)$ are plotted against the inverse temperature according to the eq 5 (where τ_{AD} is the lifetime of the acceptor in the presence of the donor, τ_D is the lifetime of the donor alone, E is the activation energy, k_B is the Boltzmann constant, and A is the pre-exponential factor)

$$\ln\left(\frac{1}{\tau_{AD}} - \frac{1}{\tau_D}\right) = -\frac{E}{k_B}\frac{1}{T} + \ln A \qquad (5)$$

From Figure 4 and Table 3 it can be seen that when the temperature increased, a clear shift toward a shorter lifetime (higher frequency) was obtained with the acceptors AF532 and AF546 while with the conventional FRET acceptor AF680 and with the Eu(III)-chelate alone, the lifetime remained nearly constant. We propose that this shift is due to a thermal excitation from the $^5D_0$ state to higher excited states, which increases the likelihood of the nFRET process when the temperature increases (see Theoretical Considerations). For the reactions containing acceptors, the data from the frequency-domain measurements were best fit with two lifetimes except for the AF546, that was best fit with three lifetimes. In the case of AF532, there might have been a third lifetime that was not distinguished due to lower

Table 3. Influence of Temperature on the Lifetimes of the Luminescent Compounds in the Hybridization Reaction at 560 nm (AF532/AF546), 730 nm (AF680), or 615 nm (Donor-Only Control with 9d-DTA Chelate Labeled Capture Oligonucleotide and Unlabeled Tracer Oligonucleotide)

	AF532		AF546			AF680		D only[a]
T (°C)	τ_1 (μs)	τ_2 (μs)	τ_1 (μs)	τ_2 (μs)	τ_3 (μs)	τ_1 (μs)	τ_2 (μs)	τ (μs)
5	0.65 ± 0.03	719 ± 6.4	0.52 ± 0.02	138 ± 4.4	482 ± 3.4	81 ± 6.9	366 ± 2.4	1441 ± 1.9
15	0.67 ± 0.02	466 ± 4.4	0.59 ± 0.04	97 ± 2.5	352 ± 2.1	84 ± 5.4	366 ± 2.4	1423 ± 2.1
25	0.69 ± 0.03	270 ± 3.5	0.56 ± 0.05	68 ± 1.5	244 ± 1.5	87 ± 7.5	365 ± 3.4	1382 ± 1.4
35	0.65 ± 0.03	160 ± 2.5	0.70 ± 0.05	49 ± 1.4	164 ± 1.4	72 ± 6.1	356 ± 2.6	1331 ± 0.9
45	0.76 ± 0.03	97 ± 1.6	0.66 ± 0.05	35 ± 1.0	109 ± 1.1	81 ± 5.9	347 ± 3.0	1256 ± 0.7
55	0.65 ± 0.05	56 ± 1.0	0.57 ± 0.10	26 ± 0.8	72 ± 1.0	73 ± 7.3	333 ± 4.2	1154 ± 1.2

[a] In addition there was a minor second lifetime component (604−156 μs, relative amplitude of 0.3−4%).

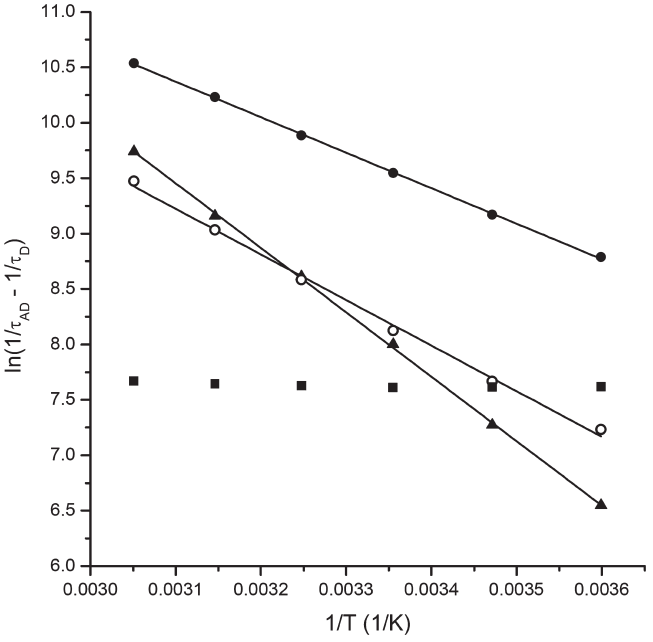

Figure 5. Logarithm of the kinetic constants ($1/\tau$) plotted against the inverse temperature for the donor−acceptor pairs in the hybridization reaction with AF532 (triangle), AF546 (circle), or AF680 (square). The closed symbols represent results fitted using the τ_2 (see Table 3), and the open symbols represent results fitted using the τ_3.

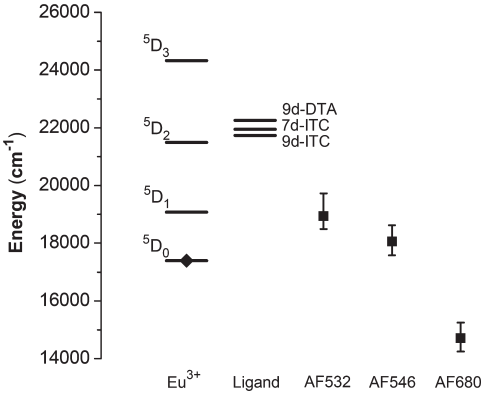

Figure 6. Simplified diagram showing the excited energy levels (from $^5D_0$ to $^5D_3$) for Eu^{3+} ion,[24] the lowest triplet states of the used light-harvesting ligands (9d-DTA, 9d-ITC, and 7d-ITC)[25] and the excitation bands for Alexa Fluor dyes (AF532, AF546, and AF680). The diamond represents the prevalent radiative energy level of the Eu^{3+} ion. The squares mark the excitation maxima of the dyes, and the error bars mark the half-width of the excitation spectrum.

signal levels resulting in the weak signal being buried in the noise. With the control sample containing the 9d-DTA chelate conjugated oligonucleotide alone there was one predominant lifetime and a second very minor component. The observed second lifetime is probably the result of the sample containing some minor impurity. The relative amplitudes for the reactions containing AF532 were approximately 80% and 20% for τ_1 and τ_2 respectively and for AF680 approximately 10% and 90%. The relative amplitudes for the reactions containing AF546 were approximately 30%, 15% and 55% for τ_1, τ_2 and τ_3 respectively. The signal intensity decrease with all the samples in Figure 4 is suspected to be the result of increased vibrational quenching by OH-groups due to the more efficient replacement of ligand coordination sites with water molecules as the temperature increases. Figure 5 shows the logarithm of the kinetic constant ($1/\tau$) plotted against the inverse temperature ($1/T$) for the different donor−acceptor pairs. From the slope of the line, the activation energy can be calculated. The obtained activation energies were 4045 ± 35 cm^{-1} (correlation coefficient R = 0.9999) for the AF532 and 2861 ± 77 cm^{-1} (R = 0.9986) or 2228 ± 20 cm^{-1} (R = 0.9998) for the AF546 (calculated based on the longest or second longest lifetime estimates respectively) with 95% confidence. The values of the pre-exponential factor A were 8.7 × 10^{11}, 3.5 × 10^9, and 6.6 × 10^8, respectively.

Theoretical Considerations. A simplified diagram depicting the energy levels for Eu^{3+} ion,[24] the lowest triplet states of the used light-harvesting ligands, and the excitation bands for Alexa Fluor dyes is shown in Figure 6. The diamond represents the lowest radiative energy level of the Eu^{3+} ion. The lowest triplet states were 22 250, 21 740, and 21 950 cm^{-1} for the 9d-DTA, 9d-ITC, and 7d-ITC ligands, respectively[25] (the exact values may differ slightly from the values indicated in the reference due to small differences in the chelate structure). The energy levels of the used dyes (AF532, AF546, and AF680) are not as well-defined as the energy levels of lanthanide ions and therefore are depicted as excitation maxima together with the half-widths of the excitation spectra.

Energy-transfer from a ligand to a lanthanide ion mainly occurs from the lowest triplet state of the ligand via a suitable accepting energy level of the ion (typically $^5D_1$ or $^5D_2$ for europium) to the lowest radiative energy level of the ion

($^5D_0$ for europium).[26] The downhill transition between the ^5D_J states is due to the rapid vibration-mediated nonradiative relaxation that deactivates more highly excited states to the radiative energy level that has the largest energy gap to the next lower level.[27] If a suitable acceptor is nearby, the energy can be further transferred to the acceptor. In conventional FRET the excitation of the acceptor is at lower energy levels than the lowest radiative energy level of the lanthanide ion. This is also true for the Eu−AF680 pair as can be seen from the energy level diagram. However, the excitation for AF532 and AF546 lies above the $^5D_0$ energy level and indicates a different energy-transfer mechanism. The $^5D_3$ and higher energy levels were not considered as possible energy-donating states because they lie above the lowest triplet state of the ligands.

One hypothesis is that nFRET is essentially a property of the lanthanide ion, not the ligand or the acceptor. Thus the observation that the nFRET phenomenon has been reported with europium and samarium,[7] but not with terbium could be explained by the ionic energy levels of terbium being unsuitable for this energy transfer mechanism. The long lifetime of the energy-transfer enhanced emission also supports the role of the lanthanide ion in the process. Laitala and Hemmilä have proposed that the nFRET phenomenon with europium is related to different energy-transfer processes from the upper $^5D_1$ and $^5D_2$ energy levels of the Eu^{3+} ion.[6] One presumable mechanism for the nFRET phenomenon could be the already previously studied energy transfer mechanism through thermal excitation[20,28,29] that leads to the population of the higher ionic energy states above the radiative energy level. Hyppänen et al.[20] have studied the energy levels and transitions of europium chelates including the thermal excitation from $^5D_0$ to $^5D_1$. This effect can also be seen in the inset of Figure 2 as the weak long-living emission peaks around 530−560 nm. These emission bands are the result of energy transferring from the triplet state of the ligand via the higher accepting energy states to the $^5D_0$ state and from there by the thermal excitation to the $^5D_1$ state. The $^5D_0$ to $^5D_1$ states of europium are energetically very close to each other, the difference being approximately 1700 cm^{-1} which facilitates the thermal excitation. However, the activation energies obtained in this work for the AF532 and AF546 were greater than 1700 cm^{-1}, and thus it is possible that the energy is transferred from $^5D_0$ to an energy level higher than $^5D_1$.

An alternative explanation for the observed activation energies could be the presence of a ligand-to-metal charge-transfer state (CTS) proposing that nFRET would be a property of the light harvesting ligand. The observation that the nFRET phenomenon has been reported with europium and samarium, but not with terbium could thus be explained by the oxidation states of terbium being unsuitable for charge transfer through this mechanism (terbium cannot be reduced to +2 oxidation stage like europium and samarium). An et al.[30] were able to separate the lifetime of the $^5D_1$ state of an Eu-doped Gd(III) diketonate into temperature dependent and independent contributions. From these the temperature independent lifetime was attributed to carbonyl-mediated relaxation and the temperature dependent lifetime to a low-lying ligand-to-metal CTS. The open question in this hypothesis is why the hybridization reactions containing AF532 and AF546 gave different activation energies even though the same ligand was used in both experiments.

In all measurements a conventional FRET acceptor AF680 was used as a control with the same donor conjugates as with the nFRET acceptors to rule out any false effects originating from the ligand or the linkers. Since the only difference between the nFRET and FRET reactions was the acceptor molecule, such effects as the direct interaction of the light harvesting ligand with the acceptor fluorophore (contact-induced transfer mechanism) are highly unlikely and could be ruled out. Also the melting temperature of the oligonucleotides, that is the temperature at which half of complementary oligonucleotides are in a double helix state, was so high (approximately 90 °C), that the heating was not presumed to cause any effect, and accordingly no effect was seen in the control with the AF680 acceptor.

CONCLUSIONS

In this study we have demonstrated for the first time a difference in the distance and temperature dependency between conventional (Förster-type) and nonoverlapping FRET by using a homogeneous DNA-hybridization assay and frequency-domain lifetime measurements. Both methods utilized capture oligonucleotides labeled at the 5′-end with a Eu(III)-chelate that hybridized to tracer oligonucleotides labeled with short-lifetime organic fluorophore labels at various distances from the 3′-end. In the homogeneous hybridization assay a plate reader with time-resolution mode was used to collect information on the energy-transfer enhanced emission and the energy-transfer efficiencies at different donor−acceptor distances were calculated. In the lifetime measurements varying temperature was used to monitor the effect of temperature on the energy-transfer signal utilizing a modular FD luminometer.

From the energy transfer efficiency measurements it could be seen that the nFRET mechanism resulted in very efficient energy transfer despite the lack of spectral overlap, but only at short distances. Even though theoretical calculation of the Förster radius gives rational values regardless of extremely small spectral overlap, conventional FRET theory cannot solely explain the observed efficient energy transfer with the nFRET acceptor. Unlike conventional FRET, nFRET also showed clear temperature dependency. Based on our measurements, we propose that in nFRET a thermal excitation occurs from the lowest radiative $^5D_0$ state of the ion to higher excited states, either ionic or associated with a ligand-to-metal CTS. From the higher energy state the energy further transfers to the acceptor, provided that the donor−acceptor distance is sufficiently short.

The distance dependency of nFRET is understandable considering that the energy transfer from the upper energy states of europium via the thermal excitation mechanism has to compete with the conventional FRET mechanism where the energy transfer to the $^5D_0$ state is very fast (in the microsecond range). The temperature effect on the nFRET lifetime seen in the FD measurements can, on the other hand, be understood considering that the energy states involved in the mechanism are separate entities having their own time dependent "population densities", and the heating of the reaction shifts the population density from the $^5D_0$ state toward the higher energy states thus increasing nFRET efficiency. What comes to the exact mechanism, there are still open questions which warrant further studies of nFRET by applying the frequency-domain methods on new acceptors and donors including also Tb(III) and Sm(III) complexes.

On the application side nFRET provides some distinct advantages. In nFRET, the energy-transfer enhanced emission of the acceptor is measured at shorter wavelengths than where the emission of the donor is observed. This reduces the donor background when measuring the energy-transfer enhanced

acceptor signal and so improves the detection sensitivity. By using a suitable nFRET acceptor in the hybridization assay, 10-fold higher signal-to-background ratios were achieved compared to reactions using an acceptor strictly following the Förster theory. The possibility of using spectrally nonoverlapping acceptors in energy-transfer assays also widens the range of applicable fluorophores with favorable characteristics. Thus the use of nFRET labels paves the way for new and increasingly sensitive assay applications.

■ ASSOCIATED CONTENT

Supporting Information. Spectral measurements of the energy-transfer reactions, as well as determination of the quantum yield of the Eu(III)-chelates. This material is available free of charge via the Internet at http://pubs.acs.org.

■ AUTHOR INFORMATION

Corresponding Author

*Phone: +358-2-333-8572. Fax: +358-2-333-8050. E-mail: johanna.vuojola@utu.fi.

Author Contributions

§These authors contributed equally to this work.

■ ACKNOWLEDGMENT

This study was supported by Tekes, the Finnish Funding Agency for Technology and Innovation and by the Academy of Finland (Grant Nos. 119497 and 140758).

■ REFERENCES

(1) Förster, T. *Ann. Phys.* **1948**, *2*, 55–75.
(2) Stryer, L.; Haugland, R. P. *Proc. Natl. Acad. Sci. U.S.A.* **1967**, *58*, 719–726.
(3) Hemmilä, I.; Laitala, V. *J. Fluoresc.* **2005**, *15*, 529–542.
(4) Clegg, R. M. *Methods Enzymol.* **1992**, *211*, 353–388.
(5) Stryer, L. *Annu. Rev. Biochem.* **1978**, *47*, 819–846.
(6) Laitala, V.; Hemmilä, I. *Anal. Chem.* **2005**, *77*, 1483–1487.
(7) Laitala, V.; Hemmilä, I. *Anal. Chim. Acta* **2005**, *551*, 73–78.
(8) Vuojola, J.; Lamminmäki, U.; Soukka, T. *Anal. Chem.* **2009**, *81*, 5033–5038.
(9) Mathis, G. *Clin. Chem.* **1995**, *41*, 1391–1397.
(10) Hemmilä, I. *J. Alloys Compd.* **1995**, *225*, 480–485.
(11) Dickson, E. F.; Pollak, A.; Diamandis, E. P. *J. Photochem. Photobiol., B* **1995**, *27*, 3–19.
(12) Kokko, T.; Kokko, L.; Soukka, T.; Lövgren, T. *Anal. Chim. Acta* **2007**, *585*, 120–125.
(13) Morrison, L. E. *Anal. Biochem.* **1988**, *174*, 101–120.
(14) Lakowicz, J. R. *Principles of Fluorescence Spectroscopy*, 3rd ed.; Springer: New York, 2006; Chapter 5.
(15) Kankare, J.; Hyppänen, I. *Lanthanide Luminescence: Photophysical, Analytical and Biological Aspects. Springer Series on Fluorescence*; Hänninen, P., Härmä, H., Eds.; Springer Verlag: Berlin, 2011; Vol. 7, pp 279−312.
(16) Cardullo, R. A.; Agrawal, S.; Flores, C.; Zamecnik, P. C.; Wolf, D. E. *Proc. Natl. Acad. Sci. U.S.A.* **1988**, *85*, 8790–8794.
(17) Mukkala, V.-M.; Helenius, M.; Hemmilä, I.; Kankare, J.; Takalo, H. *Helv. Chim. Acta* **1993**, *76*, 1361–1378.
(18) von Lode, P.; Rosenberg, J.; Pettersson, K.; Takalo, H. *Anal. Chem.* **2003**, *75*, 3193–3201.
(19) Takalo, H; Mukkala, V.-M.; Mikola, H.; Liitti, P.; Hemmilä, I. *Bioconjugate Chem.* **1994**, *5*, 278–282.
(20) Hyppänen, I.; Soukka, T.; Kankare, J. *J. Phys. Chem. A* **2010**, *114*, 7856–7867.
(21) Dexter, D. L. *J. Chem. Phys.* **1953**, *21*, 836–850.
(22) Selvin, P. R.; Rana, T. M.; Hearst, J. E. *J. Am. Chem. Soc.* **1994**, *116*, 6029–6030.
(23) Selvin, P. R. *IEEE J. Sel. Top. Quantum Electron.* **1996**, *2*, 1077–1087.
(24) Carnall, W. T.; Fields, P. R.; Rajnak, K. J. *Chem. Phys.* **1968**, *49*, 4450–4455.
(25) Latva, M.; Takalo, H.; Mukkala, V.-M.; Matachescu, C.; Rodriguez-Ubis, J. C.; Kankare, J. *J. Lumin.* **1997**, *75*, 149–169.
(26) Soini, E.; Lövgren, T. *Crit. Rev. Anal. Chem.* **1987**, *18*, 105–154.
(27) Werts, M. H. *Sci. Prog.* **2005**, *88*, 101–131.
(28) Kropp, J. L.; Dawson, W. R. *J. Chem. Phys.* **1966**, *45*, 2419–2420.
(29) Haas, Y.; Stein, G. *Chem. Phys. Lett.* **1971**, *8*, 366–368.
(30) An, Y.; Schramm, G. E.; Berry, M. T. *J. Lumin.* **2002**, *97*, 7–12.